Journal of
Materials Chemistry B

Materials for biology and medicine

Accepted Manuscript

This article can be cited before page numbers have been issued, to do this please use: S. Taheri, R. B. Doshi, A. K. Nguyen, S. Islam, J. Mata, J. Ruan, R. Tilley and K. Kilian, *J. Mater. Chem. B*, 2026, DOI: 10.1039/D6TB00490C.

ROYAL SOCIETY OF CHEMISTRY

rsc.li/materials-b

Hierarchical Stabilization of Bioactive Hydrogels by Multi-Arm Peptide–Polymer Supramolecular Staples

View Article Online
DOI: 10.1039/D6TB00490C

Somayeh Taheri[1], Md Shariful Islam[1], Riddhesh Bhadresh Doshi[1], Jitendra Mata[1,2], Ashley K. Nguyen[1], Juanfang Ruan[3], Richard Tilley[1,3], Kristopher A. Kilian[1,3,4]*

[1]School of Chemistry, Australian Centre for NanoMedicine, University of New South Wales Sydney, New South Wales, Australia

[2]Australian Centre for Neutron Scattering, Australian Nuclear Science and Technology Organization, Lucas Heights, NSW, 2234, Australia

[3]Electron Microscope Unit, Mark Wainwright Analytical Centre, University of New South Wales (UNSW Sydney), Sydney, NSW 2052, Australia

[4]School of Materials Science and Engineering, University of New South Wales (UNSW), Sydney, New South Wales, Australia

**Corresponding Author:* k.kilian@unsw.edu.au

Abstract

Supramolecular peptide hydrogels offer attractive bioactivity and dynamic mechanical behavior for three-dimensional cell culture and tissue engineering. However, their broader use is often limited by slow gelation and insufficient mechanical stability. Here, we introduce a molecular design strategy in which a tryptophan zipper pendant multiarm poly (ethylene glycol) (Trpzip-PEG) conjugate is incorporated into Trpzip nanofibrillar hydrogels to facilitate hierarchical tuning of materials properties. Trpzip peptides self-assemble into entangled nanofiber networks, while the addition of Trpzip-PEG conjugate induces reorganization of these assemblies. Electron microscopy and neutron scattering reveal the formation of shorter, more densely bundled fibers with increased microporosity and a fractal network architecture, suggesting that the conjugate acts as a supramolecular "staple". These structural changes markedly accelerate gelation and increase stiffness, yield behavior, and thixotropic recovery. Importantly, the Trpzip/Trpzip-PEG supramolecular hybrid hydrogels remain cytocompatible, support adipose-derived stem cell adhesion, viability, and proliferation over time. Together, these findings demonstrate that Trpzip/Trpzip-PEG hybrid hydrogels offer a versatile platform for engineering mechanically robust yet bioactive soft materials for 3D cell culture, biofabrication, and regenerative medicine applications.

Introduction

Native tissue extracellular matrices (ECMs) consist of complex three-dimensional networks of macromolecules derived primarily from amino acids and saccharide building blocks. These

interconnected and hierarchical structures provide both structural support and biochemical cues that regulate essential cellular processes, including proliferation, migration and morphogenesis (1–3). To evaluate these functions in vitro, highly hydrated polymer networks (hydrogels) have been designed to mimic key ECM characteristics, and are now widely used in biomedical applications such as cell culture, tissue engineering, and drug delivery (4–6). Hydrogels possess desirable properties for ECM mimicry, including biocompatibility, viscoelastic compliance, and multiscale porosity (7,8). Recent advances have further expanded their functionality through the incorporation of stimuli-responsive features and interpenetrating polymer networks (9,10).

Peptide-based supramolecular systems, developed through both synthetic and recombinant approaches, offer precise control over molecular design, enabling tunable self-assembly and biofunctionality (11,12). Synthetic peptides can be tailored with defined sequences (e.g., coiled-coil or β-sheet motifs) to promote hierarchical organization, while recombinant techniques allow scalable production and incorporation of biologically active motifs such as RGD cell-adhesion sequences (13,14). The self-assembly of peptide nanofibers is governed by a range of noncovalent forces, including hydrophobic interactions, electrostatic attraction, hydrogen bonding, π–π interactions, and van der Waals forces, which collectively stabilize low-energy supramolecular assemblies. Environmental factors such as pH, ionic strength, and assembly kinetics further influence this process (15,16). Secondary structural motifs, including α-helices, β-sheets, and β-hairpins play a central role in defining the three-dimensional architecture and function of peptide assemblies (17).

Hydrogels formed from self-assembling peptides exhibit several advantages, including injectability, reversible gelation through noncovalent interactions, and the capacity to recover mechanical strength following deformation. These features, combined with inherent biocompatibility and enzymatic degradability into natural amino acids, make them highly versatile for biomedical applications (6,18). In addition, their well-defined fibrillar networks provide tunable stiffness and dynamic viscoelastic behaviors such as shear-thinning and self-healing, closely resembling native ECM mechanics (6,18,19). Despite these advantages, purely peptide-based hydrogels often suffer from limited mechanical robustness due to the relatively weak non-covalent interactions that stabilize the networks well as limited bioactivity compared to natural matrices (20,21). To overcome these limitations, recent approaches have focused on hybrid systems that integrate peptide nanofibers with polymer networks and polymer-peptide conjugates, or supramolecular cross-linkers, thereby enhancing mechanical robustness while introducing biologically relevant cues. However, many of these hybrid strategies rely on permanent covalent networks or dense polymer matrices, which can restrict the dynamic, adaptive behaviour that makes supramolecular peptide hydrogels attractive in the first place (22,23).

Tryptophan zipper (Trpzip) hydrogels have emerged as a promising class of short peptide-based materials that self-assemble into microporous fibrillar networks with inherent bioactivity to resident cells (2,24). Although these self-assembled peptide networks display useful mechanical attributes like self-healing and stress relaxation, they remain relatively weak, with low yield points that limit their broader applicability. Recent studies have demonstrated that hybridization strategies can substantially improve Trpzip hydrogel performance. Liu et al. demonstrated that co-assembly of Trpzip peptides with a covalent PEG network significantly improved hydrogel stiffness, toughness, and cell adhesion (25). Similarly, Doshi et al. combined Tripzip motifs with gellan gum to achieve rapid gelation, collagen-like viscoelasticity, and enhanced cell viability (26).

In this paper, we present a molecular design approach to tune the biophysical properties of Trpzip/Trpzip-PEG hydrogels through incorporation of a Trpzip terminated multi-arm polyethylene glycol (Trpzip-PEG) conjugate. This multivalent architecture is designed to reinforce supramolecular network connectivity by enabling simultaneous interactions with multiple Trpzip nanofibers, without relying on permanent covalent cross linking that could compromise the dynamic nature of the peptide assembly. The addition of this multi-arm PEG-based molecule (Trpzip-PEG conjugate) accelerates gelation and leads to increased stiffness, higher yield-point, and improved recovery following mechanical fracture, while maintaining bioactivity that promotes cell adhesion and proliferation. Electron microscopy and neutron scattering analysis suggest that the multiarm Trpzip-PEG conjugate acts as a supramolecular “staple”, effectively linking Trpzip nanofibers, thereby mechanically stabilizing the overall network. This modular and tunable supramolecular approach provides a versatile platform for diverse applications spanning 3D cell culture, therapeutic delivery and tissue engineering.

Results and discussion

Peptide-PEG conjugates modulate hydrogel network morphology through structural (re)organization

Trpzip hydrogels show innate bioactivity, with unique mechanical properties like tunable yield point, self-healing and stress relaxation behavior (2). However, the assembly mechanism imparts poor mechanical properties that render it unsuitable for some biomaterials and tissue engineering applications. In particular, the slow gelation kinetics obviates use in applications requiring rapid formation, such as wound sealing, while low yield stress limits load bearing applications such as tissue implants. Previous work suggested that these mechanical limitations arise from hierarchical organization of the network, where nanofiber bundles assemble into microscale aggregates that are only loosely associated with one another (2). We therefore reasoned that introducing a supramolecular Trpzip-terminated linker could stabilize Trpzip nanofibers and reinforce inter bundle connectivity.

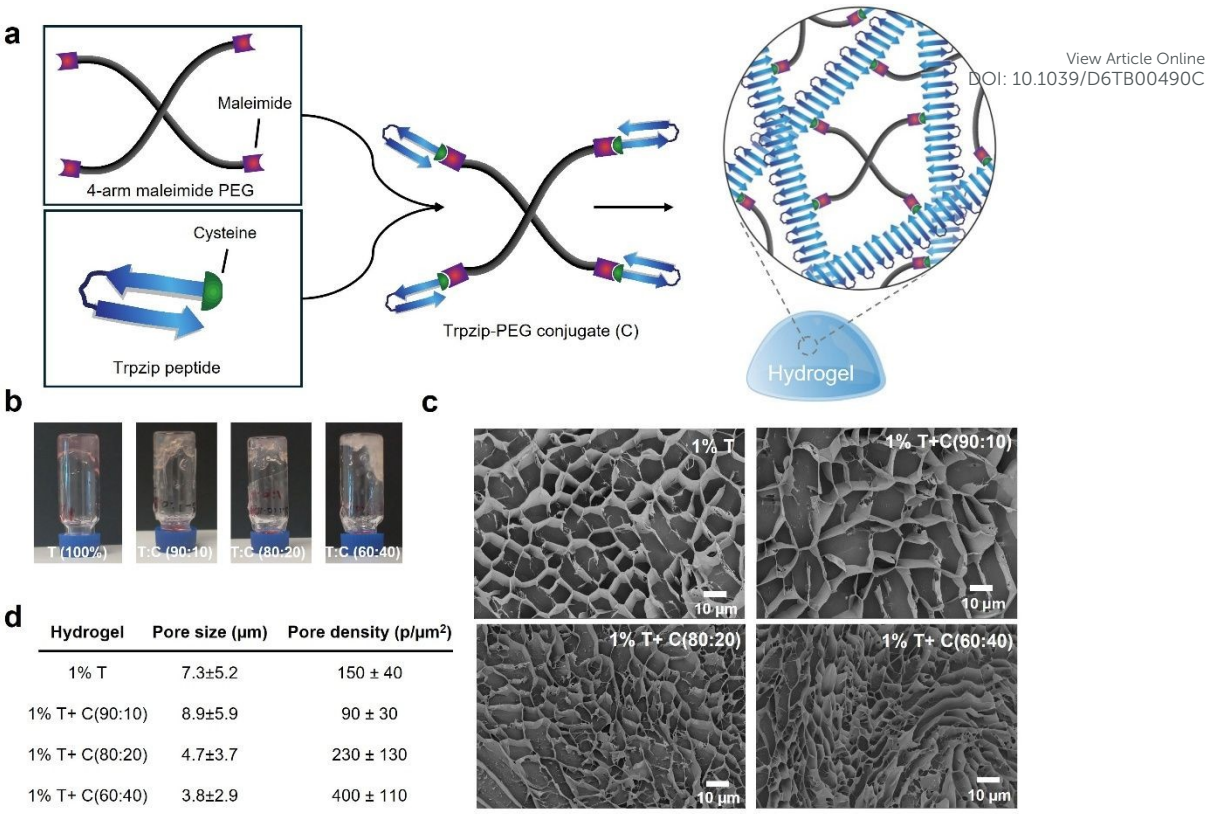

d

Hydrogel	Pore size (µm)	Pore density (p/µm²)
1% T	7.3±5.2	150 ± 40
1% T+ C(90:10)	8.9±5.9	90 ± 30
1% T+ C(80:20)	4.7±3.7	230 ± 130
1% T+ C(60:40)	3.8±2.9	400 ± 110

Fig. 1 Schematic, and characterization of Trpzip-based hydrogels. a Schematic illustration of the route followed to form Trpzip/Trpzip-PEG conjugate supramolecular hybrid hydrogels. **b** The gelation of Trpzip/Trpzip-PEG conjugate supramolecular hybrid hydrogels at pH 7 in DMEM. **c** Cryo-Scanning electron microscope (cryo-SEM) images of the structure of Trpzip-based hydrogels, presenting porous structure (scale bar = 10 µm): **d** pore size and pore density of 1% (w/v) Trpzip and its Trpzip-conjugate hydrogels.

The Trpzip–PEG conjugate is covalently bonded macromolecule, with network formation occurring through non-covalent interactions between the peptide-terminated PEG and the peptide nanofibers, resulting in a hybrid supramolecular system (**Fig. 1a**). To test this idea, we designed a conjugate between a cysteine terminated Trpzip peptide and 4-arm PEG-maleimide (PEG-MAL, 20 kDa). PEG-MAL was chosen due to its hydrophilicity, biocompatibility, and the multi-arm (star) architecture, which provides four reactive sites per macromolecule. Conjugation was carried out through Michael addition between the cysteine thiol and the maleimide group (**Fig. S1**) (27). Successful coupling was confirmed by ^{1}H NMR spectroscopy, which showed disappearance of the maleimide hydrogen singlet peak at around 6.9 ppm (**Fig. S2**) (27). To evaluate the influence of Trpzip-PEG conjugate on gel formation, Trpzip-PEG dissolved in buffer or culture media was mixed with Trpzip peptide dissolved in water to yield a final concentration of 1% (w/v), with Trpzip: Trpzip-PEG ratios of 90:10, 80:20 and 60:40 (**Table S1**). It should be noted that the reported concentrations refer to Trpzip peptide content, and that the total solids content increases with increasing Trpzip–PEG fraction. The selected Trpzip:Trpzip–PEG ratios (90:10, 80:20, and 60:40) were chosen to systematically investigate the effect of increasing conjugate content while maintaining a continuous peptide network as the primary structural component, enabling progressive modulation of supramolecular organization without

disrupting peptide self-assembly. After mixing thoroughly, each composition was subjected to inversion tests as a qualitative assessment of gelation. Each formulation resulted in a stable gel with evidence for enhanced gelation upon inclusion of the Trpzip-PEG macromer (**Fig. 1b**). The Trpzip–PEG conjugate alone did not form a self-supporting hydrogel under the conditions studied, indicating that gelation is driven by peptide self-assembly, with the conjugate acting to modulate network organization rather than forming an independent gel.

To investigate the morphological characteristics of the hydrogels and assess how their microstructures changed with the addition of Trpzip-PEG, cryogenic scanning electron microscopy (cryo-SEM) was employed. Cryo-SEM sample surfaces showed an apparent porous/microporous morphology across all Trpzip-based hydrogels (**Fig. 1c**). As cryo-SEM of bulk hydrogels can be influenced by freezing and fracturing artefacts, these observations are interpreted qualitatively and used primarily for comparison between formulations. Notably, addition of the Trpzip-PEG led to changes in the apparent pore morphology, with increasing PEG content leading to denser structures and reduced feature sizes (**Fig. 1d**). This shift in microstructure is likely due to enhanced physical crosslinking between the peptide and the Trpzip-PEG conjugate, suggesting increased intermolecular interactions and network densification.

Next, to visualize changes in nanostructure with addition of Trpzip-PEG conjugate, cryo-transmission electron microscopy (cryo-TEM) was conducted. The predominant morphology in all Trpzip-based hydrogel samples consisted of ribbon-like nanofibrous assemblies (**Fig. S3a**), which is consistent with previously reported β-hairpin-based peptide hydrogels (28,29). The overall arrangement appears to be a mix of interwoven single fibers and ribbon-like elements, suggesting the presence of both narrow and broader supramolecular assemblies within the network. Overall, the fibers in each sample appeared continuous and uniform, indicative of a robust β-hairpin self-assembly mechanism (**Fig. S3a, Movie S1-4** and **Table S2**) To further assess the presence of β-sheet-rich structures within the Trpzip and Trpzip/Trpzip–PEG hydrogels, Thioflavin T (ThT) fluorescence assays were performed (**Fig. S3b**). ThT is a benzothiazole dye that exhibits enhanced fluorescence upon binding to β-sheet-rich assemblies, and is widely used to probe amyloid-like fibrillar structures with minimal interference from other secondary conformations (30,31). As shown in **Fig. S3b**, all hydrogel formulations displayed measurable fluorescence intensity at both room temperature (RT) and 37 °C, confirming the presence of β-sheet structures consistent with the β-hairpin-driven self-assembly observed by cryo-TEM and scattering analyses. Importantly, comparison between pure Trpzip hydrogels and Trpzip/Trpzip–PEG hydrogels revealed no statistically significant differences (ns) in fluorescence intensity across all compositions and temperatures, indicating that incorporation of the Trpzip–PEG conjugate does not disrupt the underlying β-sheet formation. Instead, these results suggest that the conjugate primarily influences higher-order network organization, such as nanofiber

bundling and hierarchical assembly, without altering the fundamental peptide secondary structure. Additionally, the comparable ThT intensities observed at RT and 37 °C indicate that β-sheet formation is largely temperature-independent within this range, supporting the structural stability of the supramolecular assemblies under physiologically relevant conditions. Together, these findings reinforce that altered microstructures of the hybrid hydrogels arise from supramolecular reorganization rather than changes in β-sheet content (26). Small angle neutron scattering (SANS) was used to investigate nanostructure and hierarchical organization of the hydrogels. To quantitatively analyze the structural data, scattering from Trpzip hydrogels (0.5% w/v) were modelled using SasView. In the high-Q region, the flexible cylinder model provided the best fit for gelled hydrogels, reflecting the formation of long, flexible nanofibers during gelation (32,33). As shown in **Table S3** these nanofibers, with a measured radius of approximately 2.23 ± 0.02 nm, were so elongated that their lengths exceeded the instrument's detection limits (>1 μm), indicating significant fiber extension throughout the gelation process. In the low-Q region, the scattering was analysed using a power-law model, with a Porod exponent of 3.57 ± 0.03, consistent with rough-surfaced or surface-fractal-like structures at larger length scales. Altogether, gelation led to marked structural changes in Trpzip networks, producing flexible, highly elongated nanofibers that assemble into complex, rough-surfaced aggregates (24). Further, we evaluated the impact of adding 4-arm Trpzip-PEG on the hydrogel architecture using SANS. Compared to Trpzip-only hydrogels, all scattering profiles were described using an ellipsoidal form factor at high Q and by a power-law model at low Q (34). The power exponent decreased from 3.57 for pure Trpzip to 2.37 (Trpzip to Trpzip-PEG 90:10) to 2.38 (Trpzip to Trpzip-PEG 80:20) and 2.27 (Trpzip to Trpzip-PEG 60:40) (**Fig. 2a** and **Table S4**), consistent with a shift from rough surface-fractal-like structures toward more loosely packed, mass-fractal-like network organization. These results suggest that the addition of PEG conjugate alters Trpzip nanofiber packing at the microscale. Consistent with this, power scale increased from 0.8×10^{-4} to 1.63×10^{-4} as Trpzip-PEG weight fractions increased. Analysis further suggests that introduction of Trpzip-PEG is associated with increased nanofiber bundling, which can be described by ellipsoidal form factors at the probed length scales. Correspondingly, the fitted polar radii increased from 6.76±0.03 nm to 9.04±0.02 nm, whilethe equatorial radii expanded from 45.7±0.05 nm to 58±0.04 nm. The ellipsoid scale also increased from 6.1×10^{-4} to 8.15×10^{-4}, consistent with an increased degree of bundle formation (**Fig. 2a** and **Table S4**). Overall, this data indicates that modest additions of Trpzip-PEG conjugate influence the nanostructure and hierarchical assembly of Trpzip/Trpzip-PEG hydrogels.

It is tempting to speculate that the Trpzip-PEG macromer is acting as a binder to facilitate nanofiber bundling, aligned with our initial hypothesis of a supramolecular "staple". Ultra Small Angle neutron scattering (USANS) was used to analyse the micron-scale structures of Trpzip/Trpzip-PEG hydrogels.

As the weight ratio of Trpzip-PEG t35o Trpzip increased from 10:90 to 40:60, the scattering intensity correspondingly increased, indicating a higher abundance of microstructures within the 0.4–17.9 μm size range. Fitting the scattering profiles with a power-law model revealed a slight increase in the Porod exponent from 2.98 to 3.07, suggesting a shift between mass-fractal–like structures and rough surface–fractal aggregates (**Fig. 2b** and **Table S5**). These findings contribute to a deeper understanding of the material's internal architecture and its potential impact on macroscopic properties.

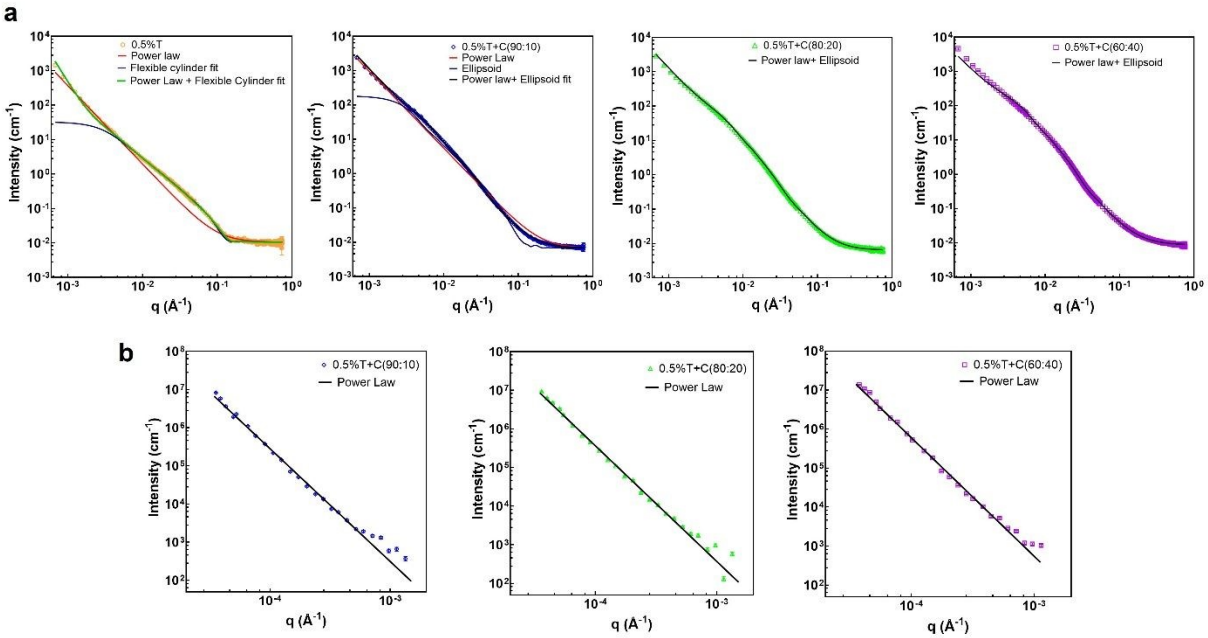

Figure 2. Scattering behaviour of Trpzip and Trpzip–PEG hydrogels. a Small-angle scattering profiles of 0.5% Trpzip in DMEM–D_2O fitted with a combined flexible-cylinder and power-law model, together with scattering profiles of 0.5% Trpzip/Trpzip–PEG hydrogels (90:10, 80:20 and 60:40 formulations) in DMEM–D_2O fitted with a combined ellipsoid and power-law model (left to right). **b** Ultra-small-angle neutron scattering (USANS) profiles of Trpzip/Trpzip–PEG hydrogels in DMEM–D_2O with power-law fits for the 90:10, 80:20 and 60:40 Trpzip:Trpzip–PEG conjugate formulations (left to right).

Trpzip-PEG addition accelerates gelation and enhances mechanical durability and self-healing. To evaluate the effect of Trpzip-PEG macromer supplementation on hydrogel mechanical properties, we used in situ oscillatory parallel plate rheometry. Increasing the pure Trpzip hydrogels from 0.5 - 2% (w/v) leads to higher storage modulus with similar gelation times (**Fig. 3; left** and **Fig. S4a**). Across all Trpzip concentrations tested, incorporation of small amounts of conjugated materials (e.g., Trpzip to Trpzip–PEG 90:10) results in a marked increase in modulus with faster gelation times. In addition to modulus, we calculated the yield point of each material, defined as the strain at which the storage modulus (G′) begins to deviate from its linear viscoelastic plateau during strain sweep measurements, indicating the onset of network yielding. At Trpzip concentrations of 0.5%, 1%, and

View Article Online
DOI: 10.1039/D6TB00490C

2% w/v, storage modulus (G′) increased by approximately 1.8-fold, 1.6-fold, and 1.8-fold, respectively, following addition of the conjugate. More notably, the

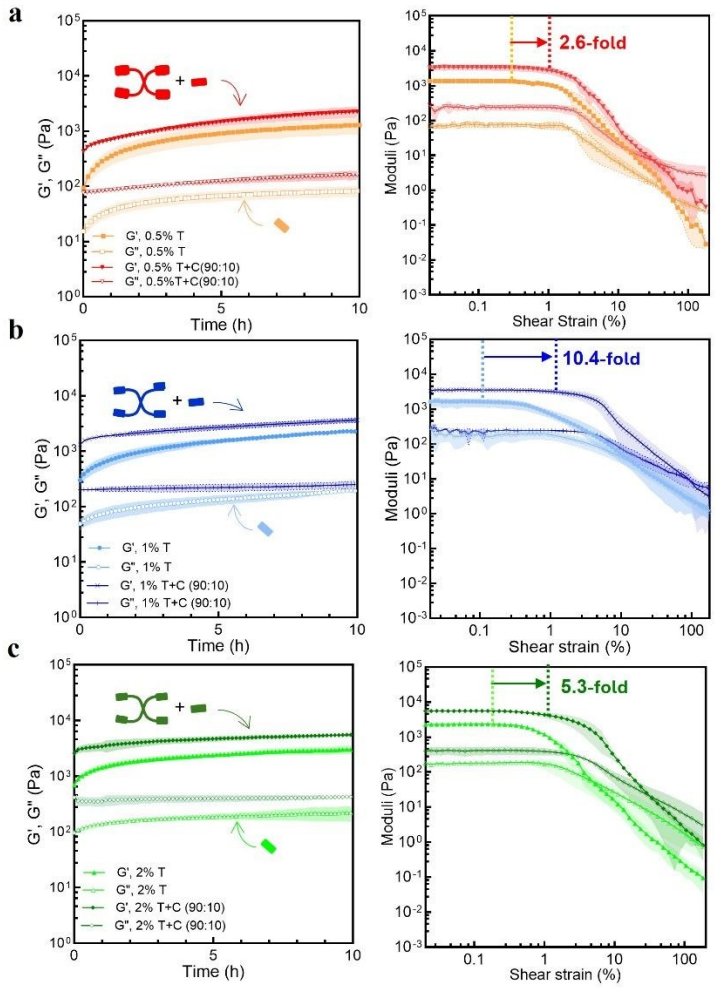

Fig. 3. Mechanical properties of Trpzip-PEG supramolecular hydrogels compared to Trpzip single network hydrogels. Oscillatory time sweeps (left sides) and strain sweeps (right sides) tests were performed at 1 Hz on **a** 0.5% w/v, **b** 1% w/v and **c** 2% w/v of Trpzip-based hydrogels. All tests were conducted in triplicate (n = 3).

yield point increased markedly at 1% and 2% concentrations (2.6-fold and 10.4-fold, respectively), while at 0.5% the difference was less pronounced, likely due to the lower modulus and increased sensitivity to measurement fluctuations at low stresses.

Consistent with these trends, **Fig. 4a** and **Fig. S4b** indicate that increasing the Trpzip–PEG conjugate concentration markedly enhances stiffness and accelerates gelation. Shear strain sweep measurements further indicated that the addition of Trpzip-PEG conjugates significantly enhanced the yield strain of the hydrogels, with increase of 8.9-fold (90:10), 6.5-fold (80:20) and 10.1-fold (60:40) compared to Trpzip hydrogels without the conjugate (**Fig. 4 b-d**). These results suggest the formation of a more stable, gel-like structure with enhanced stiffness and yielding behavior, likely due to an increased physical crosslinking or nanofiber entanglement, in line with the structural changes observed by

SANS/USANS experiments. Interestingly, the magnitude of the change is comparable across all Trpzip-PEG ratios, suggesting that it only takes a small fraction of conjugate to stabilize the materials.

In addition to the enhanced yield behavior, incorporation of the Trpzip–PEG conjugate led to a pronounced increase in hydrogel viscosity while preserving the intrinsic shear-thinning behavior of Trpzip networks (**Fig. 4Sc**). This indicates that the conjugate reinforces the network without compromising its adaptive flow response under shear. Furthermore, all compositions exhibited tunable stress-relaxation behavior as a function of conjugate content (**Fig. 4Sd, e**). Notably, the stress-relaxation half-life increased from 354 s for pure Trpzip to 980 s for the Trpzip/Trpzip-PEG (60:40 w/w) hydrogel, reflecting a slower network rearrangement consistent with increased cross-link density and enhanced viscoelastic stability. Among the tested formulations, the 60:40 ratio showed the most pronounced increase in mechanical performance within the tested range. While the origin of this trend is not yet clear and requires further investigation, the observed improvements position these hybrid hydrogels as promising candidates for applications like biofabrication, cell delivery, tissue engineering, etc. (22).

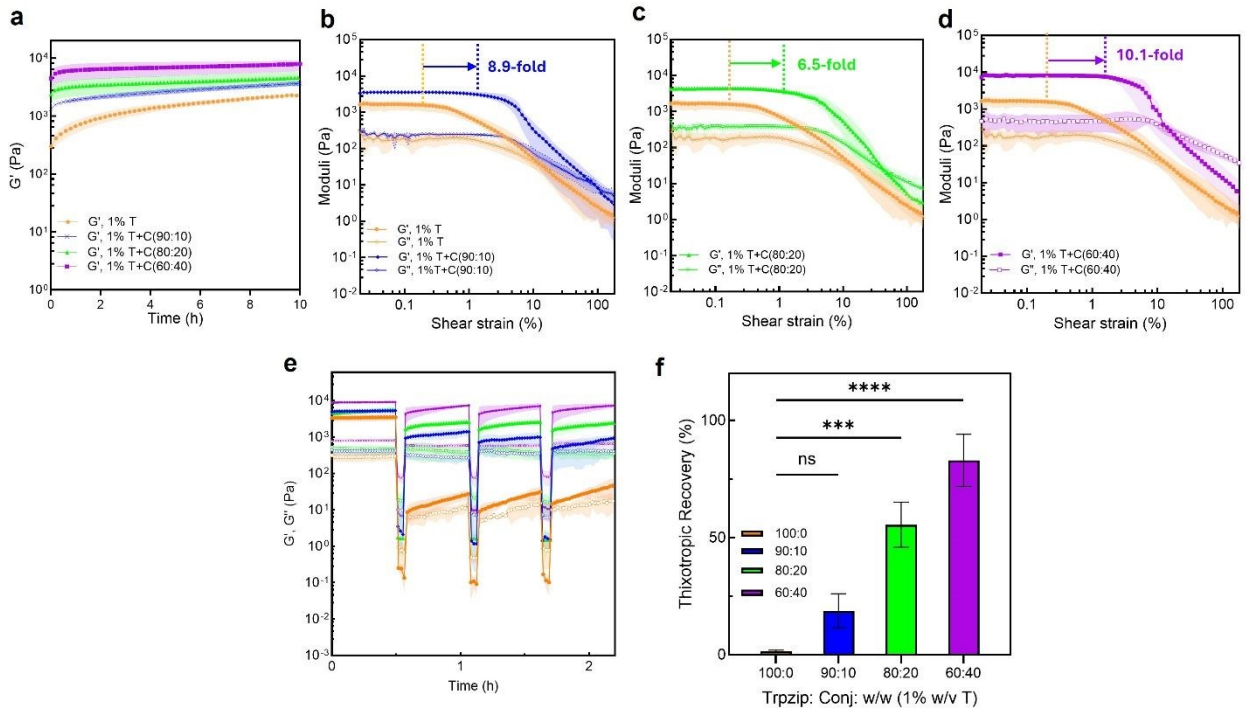

Fig. 4. Mechanical properties of 1% w/v Trpzip-based hydrogels. a Oscillatory time sweeps and **b-d** strain sweep tests of 1% w/v Trpzip hydrogel and its hydrogels with Trpzip-PEG conjugate. The dotted lines indicate yield-point. **e** Thixotropic analysis of 1% w/v Trpzip hydrogel and its hydrogels with Trpzip-PEG conjugate. **f** Thixotropic recovery of 1% w/v Trpzip-based hydrogels. All tests were conducted in triplicate (n = 3).

The Trpzip–PEG conjugate alone did not form a self-supporting hydrogel under the conditions studied, suggesting that gelation primarily depends on formation of a continuous Trpzip fibrillar network. Similar behavior has been reported in other peptide–polymer conjugate systems, where

polymer conjugation modulates supramolecular assembly but insufficient intermolecular β-sheet interactions or limited network connectivity prevent independent gel formation and instead favor finite aggregates or weakly associated structures (35–37).

One of the key attributes of peptide-based nanofiber hydrogels is the ability to recover after shear deformation, often refers to as "self-healing". To evaluate whether the addition of the Trpzip-PEG macromer would influence the self-healing characteristics of Trpzip hydrogels, we performed thixotropy experiments, where the hydrogels were subjected to high shear strain (50%), followed by recovery at low shear strain (0.1%). This cycle was repeated multiple times. Trpzip-only hydrogels showed very limited recovery, regaining only ~1.4% of the original modulus after shear, with recovery decreasing over successive cycles (approximately 99% decrease with each cycle) (**Fig. 4e, f**). In contrast, supplementation with Trpzip-PEG increased recovery to 83% of their initial modulus after shear. Importantly, each successive shear event showed comparable recovery, demonstrating how the Trpzip-PEG macromer facilitates self-healing. Similar to the increase in modulus and yield behaviour, these results suggest that the conjugate material helps reorganisation and stabilisation of the supramolecular network during thixotropic recovery. At higher applied strains (>100%), the hydrogel network exhibited extensive structural disruption with minimal recovery, indicating limited suitability for high-deformation processes such as syringe extrusion. Accordingly, the observed recovery behaviour is representative of moderate shear conditions rather than a direct demonstration of syringe-based extrusion performance. This behaviour highlights the potential of these materials in applications involving moderate shear deformation (38).

Hydrogels stabilized with the Trpzip-PEG conjugate support adipose derived stem cell (ADSC) adhesion and proliferation

Having demonstrated improved mechanical attributes with the addition of the Trpzip-PEG conjugate, we next evaluated the cytocompatibility of the hydrogels using adipose derived stem cells (ADSCs). Cells were encapsulated within the different hydrogels and cultured for 2 and 7 days, followed by fixation, immunostaining, imaging and quantitative analysis. Confocal microscopy images showed that ADSCs adhered to and spread within the Trpzip/Trpzip-PEG hydrogel matrix, indicating comparable cytocompatibility and adhesion morphology to Trpzip only hydrogels (**Fig. 5a**). Quantitative morphometric analysis demonstrated that the addition of Trpzip-PEG to Trpzip hydrogels led to notable changes in cell morphology. ADSCs cultured in Trpzip/Trpzip-PEG hydrogels exhibited a reduced aspect ratio compared to those in Trpzip-only gels, suggesting a less elongated cell shape morphology nurtured by the mixed material (**Fig. 5b-d**). Increasing the fraction of Trpzip-PEG further increased cell roundness, indicating a shift toward a more spherical morphology. These changes may reflect nanoarchitectural alterations in the hydrogel network, namely

increased nanofiber bundling and reduced effective fiber length. In addition, the presence of the conjugate may influence the physicochemical environment of the matrix, including hydration, steric effects, and cell–matrix interactions, which could also contribute to the observed changes in cell morphology. However, further imaging experiments are required to directly confirm this mechanism.

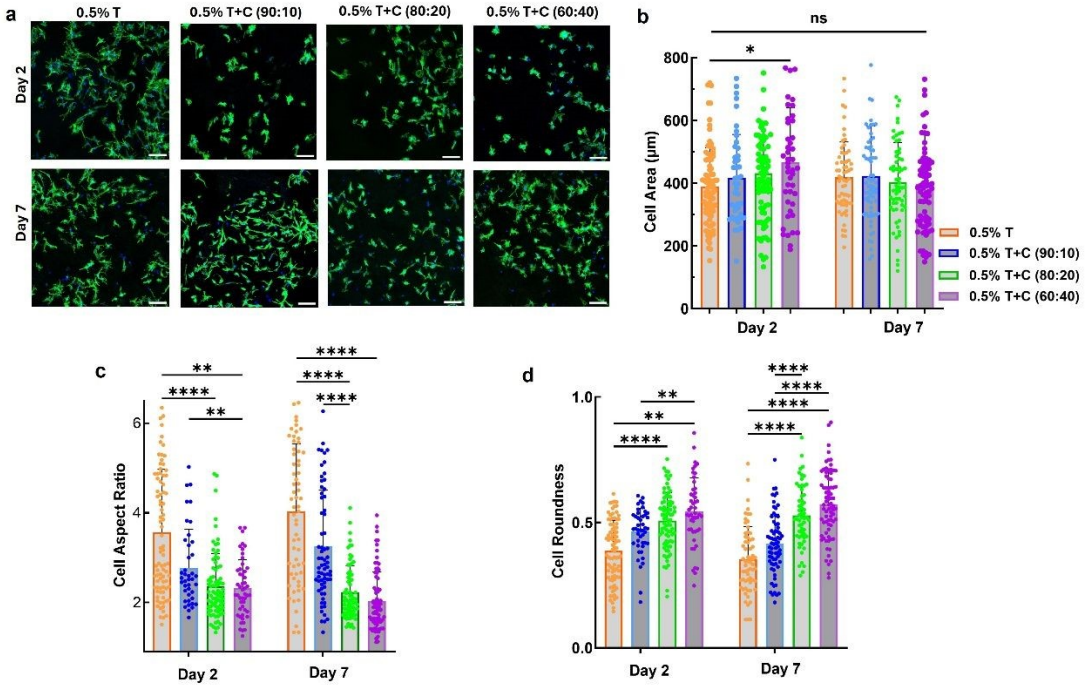

Fig. 5. Morphology and quantitative analysis of ADSCs encapsulated within Trpzip/Trpzip-PEG hydrogels at days 2 and 7. **a** Representative confocal microscopy images of adipose-derived stem cells (ADSCs) encapsulated within different Trpzip/Trpzip-PEG hydrogel formulations, stained for nuclei (DAPI, blue) and F-actin (phalloidin, green), after 2 and 7 days in culture. Scale bar: 100 μm. (b–d) Quantitative analysis of **b** cell spread area, **c** aspect ratio, and **d** roundness of ADSCs encapsulated within Trpzip/Trpzip-PEG hydrogels (n = 3). Data is presented as mean ± s.d. Statistical significance was determined using one-way ANOVA and only p values ≥ 0.05 are presented in graphs.

To explore whether Trpzip/Trpzip-PEG hydrogels support cell survival and growth over time, ADSCs were cultured for 7 days and assessed for viability and proliferation. Live/dead staining demonstrated high cell viability across all hydrogel formulations at both day 1 and day 7 (**Fig. 6a, b**). Furthermore, CyQUANT proliferation assays showed increased cell numbers over time for all materials, indicating the cytocompatibility of the hydrogels and their ability to provide a favorable microenvironment for cell survival (**Fig. 6c**). Although Trpzip/Trpzip-PEG hydrogels showed slightly reduced proliferation compared to Trpzip only gels, this trend is consistent with the observed differences in cell spreading and morphology. Overall, these results demonstrate that Trpzip/Trpzip-PEG hydrogels remain cytocompatible while allowing tuning of mechanical properties and cell adhesion behaviour, highlighting their potential for applications in regenerative medicine and tissue engineering.

View Article Online
DOI: 10.1039/D6TB00490C

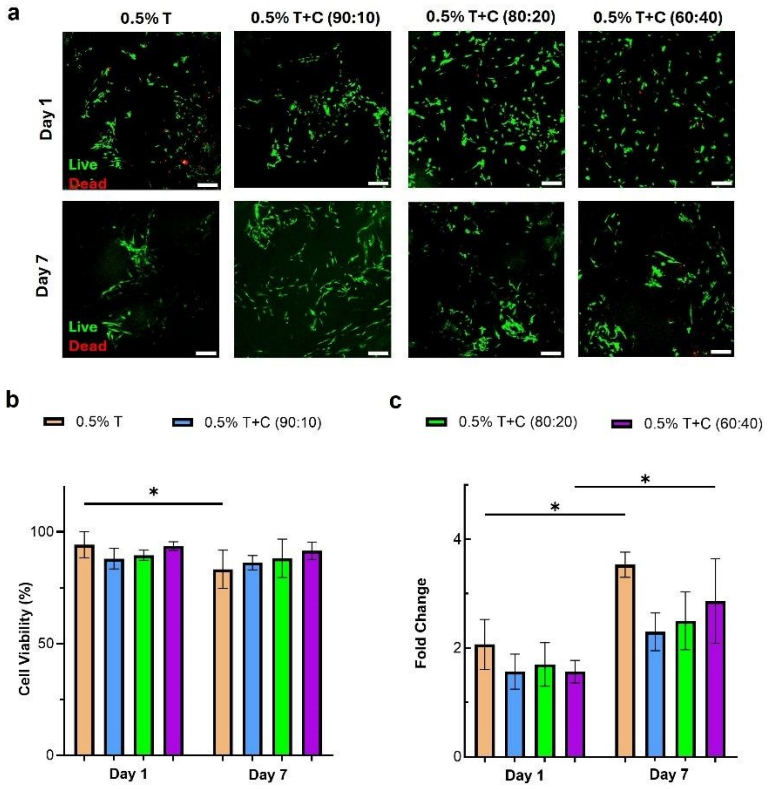

Fig. 6. Trpzip/Trpzip-PEG hydrogels support cell growth of ADSC a Confocal microscopy images of ADSCs stained with Calcein AM and ethidium homodimer in Trpzip/Trpzip-PEG hydrogels (0.5% w/v Trpzip-based hydrogels) after 1 and 7 days in culture. The Scale bar is 100 µm. **b** Quantified percentage of cell viability of ADSC cultured in 0.5% w/v Trpzip/Trpzip-PEG hydrogels (n = 3). Data are presented as mean ± s.d. P-values calculated using one-way ANOVA. **c** Cell proliferation of ADSC in 0.5% w/v Trpzip/Trpzip-PEG hydrogels. Cell proliferation was assessed after 1 and 7 days of culture using the CyQUANT assay. Fluorescence intensity was measured with a microplate reader, and results are presented as fold change relative to day 0. Data are shown as mean ± standard deviation (SD).

Conclusions

This work demonstrates how integrating a multi-arm Trpzip-PEG conjugate into Trpzip hydrogels provides a versatile approach to tune supramolecular network architecture, mechanical properties and cell activities. The conjugate reorganized the peptide assemblies at nano- and microscale levels, producing shorter, more bundled fibers and denser porous structures. These structural changes accelerated gelation and significantly enhanced stiffness, yield behavior, and self-healing capacity. Small-angle and ultra-small-angle neutron scattering revealed that the addition of Trpzip-PEG modulates both nanoscale packing and microscale aggregate architecture, confirming that minor adjustments in conjugate content allow precise control over network hierarchy. Importantly, the introduction of Trpzip-PEG conjugate preserved the inherent cytocompatibility of the Trpzip system. Adipose-derived stem cells remained viable, adhered, and proliferated within the hybrid matrices, demonstrating that enhanced mechanical performance does not compromise the biological responsiveness of the network. Together, these results establish Trpzip/Trpzip-PEG hybrid hydrogels as tunable, cytocompatible materials. Their combined mechanical robustness and biological support highlight their potential for applications in 3D cell culture, biofabrication, and regenerative medicine.

View Article Online
DOI: 10.1039/D6TB00490C

Methods

Materials

Synthetic peptides (Trpzip-q5) and Trpzip_q5_cys were purchased as the formate salt (purity >98%) from GenScript Biotech (Singapore) Pte Ltd and used without further purification. 4 Arm-PEG-MAL (20K) was purchased from JenKem Technology.

Conjugate synthesis and purification

Trpzip_q5_cys (GenScript) with the sequence of SWTWQGNVWTWVC and cysteine residue and 4 Arm-PEG-MAL (JenKem Technology, 20KDa) were used. 4 Arm-PEG-MAL and Trpzip were dissolved in PBS (pH = 8.0) and peptide-grade DMF respectively in separate vials at desired concentrations and then were added together. The reaction was allowed to proceed overnight at RT on an orbital shaker. The obtained conjugated material was purified by dialysis against water and freeze-dried to a fluffy solid.

Maleimides have been the most commonly utilized thiol-specific PEGylation reagents exhibiting high reactivity under mild reaction conditions, such as neutral pH (39). On the other hand, cysteines are a desirable site for polymer-protein conjugation due to their limited availability for reaction. The synthesis of Trpzip peptide- 4-arm PEG-MAL conjugate (sample code: Trpzip-PEG conjugate or briefly Trpzip-PEG) was conducted through the click chemistry, Michael addition reactions (**Fig. S1**) (36). **Fig. S2** depicts the proton nuclear magnetic resonance (^{1}H NMR) spectrum of 4 arm PEG-Mal (top) and Trpzip_q5_cys / 4-arm PEG conjugate (bottom). As can be seen disappearance of the peak at around 6.9 ppm indicates there is no maleimide left and the conjugation reaction was completed.

Hydrogel preparation

Trpzip hydrogels were prepared using positively charged Trpzip-q5 with the sequence SWTWQGNVWTWK and overall charge of +1 at pH=7 through ionic-triggered gelation, which involved dissolving lyophilized peptides in Milli-Q water on a hot plate at 40 °C using magnetic stirring, followed by the addition of high-glucose Dulbecco's modified Eagle's medium (DMEM) which has 110.34 mM NaCl, 44.04 mM NaHCO3, 1.80 mM CaCl2, 5.33 mM KCl etc. as cell culture media to achieve the desired final concentration.

In Trpzip/Trpzip-PEG hydrogels, the conjugated material was dissolved in DMEM and mixed with Trpzip peptide solution to initiate gelation. The reported weight percentage (e.g., 0.5%, 1%, 2% w/v) refers to the concentration of Trpzip peptide, which is kept constant across all formulations. The Trpzip–PEG conjugate is added relative to this fixed peptide mass at defined ratios (90:10, 80:20, and

View Article Online
DOI: 10.1039/D6TB00490C

60:40, Trpzip:Trpzip–PEG, w/w), resulting in a slight increase in total solids content with increasing conjugate fraction. The material compositions and sample codes are listed in **Table S1**.

Cryogenic Scanning Electron Microscopy (Cryo - SEM)

Trpzip and Trpzip/Trpzip-PEG hydrogel samples were loaded into cylindrical molds positioned on a cryo-SEM stub and secured to the specimen holder. Rapid freezing was achieved by immersing the holder in nitrogen slush to increase cooling rates prior to cryo-fracture and imaging. Because complete vitrification of bulk hydrogel samples is not guaranteed under these conditions, the resulting cryo-SEM images were interpreted qualitatively and in conjunction with cryo-TEM and neutron scattering data. Following freezing, the samples were transferred under vacuum into a cryo-preparation chamber (Quorum P3010T) maintained at –120 °C. Within the chamber, the hydrogels were fractured using a scalpel that had been pre-cooled to the same temperature to reveal their internal morphology. The fractured specimens were then moved to a Zeiss Crossbeam 550 FIB-SEM system for imaging. Micrographs were obtained at –120 °C using an accelerating voltage of 2 kV with secondary electron detection.

Cryo- transmission electron microscopy (Cryo-TEM)

A 4.2uL droplet of sample was applied to glow discharged copper grids (Quantifoil R2/2, Quantifoil Micro Tools) and blotted for 4.5s in a 100% humidity chamber at 4C°, with a blotting force of 3. The grids were then plunge-frozen in liquid ethane using a Vitrobot Mark IV device (Thermo Fisher Scientific). The grids were imaged using a Talos Arctica cryoTEM (Thermo Fisher Scientific), operating at 200kV with the specimen held at liquid nitrogen temperatures. Images were captured using a Falcon 3EC direct detector camera in linear mode.

The tilt series were collected with tilt range ± 60°, 2° angular increment and defocus -8.0 µm. Dose of each tilt series was 120 e/A^2. The reconstruction was done with IMOD 4.12.45 package.

Thioflavin T (ThT) Fluorescence Assay

Trpzip and Trpzip/Trpzip-PEG hydrogel samples (100 µL) were dispensed in triplicate into a 96-well flat-bottom microplate and incubated at 37 °C overnight. Subsequently, 150 µL of a 200 µM Thioflavin T solution prepared in PBS was added to each well, followed by an additional 24 h incubation period. The samples were then washed three times with 1× PBS over 24 h. After washing, the hydrogels were maintained in PBS and their fluorescence intensity was recorded using a CLARIOSTAR multimode microplate reader (BMG Labtech, Melbourne, VIC, Australia), employing excitation and emission wavelengths of 440 nm and 490 nm, respectively. Background fluorescence from ThT alone was subtracted from the readings obtained from ThT-treated hydrogel samples to normalize the data.

Small Angle Neutron Scattering (SANS)

Trpzip peptide was dissolved in D_2O to form Trpzip solution. Deuterated DMEM was prepared by dissolving lyophilized high-glucose DMEM in D_2O and Trpzip-PEG conjugate was dissolved in deuterated DMEM. Trpzip gels were prepared by mixing Trpzip solution with deuterated DMEM while Trpzip/Trpzip-PEG conjugate gels were prepared by mixing Trpzip solution with Trpzip-PEG conjugate solution. SANS measurements were performed on hydrogels samples at 37 ºC. The structure of the hydrogels was analysed using the Quokka pinhole small-angle neutron scattering instrument (40).Samples were loaded into 20 mm demountable cells with a 1 mm pathlength. Scattering data of samples were collected across a full q range of 0.0007-0.73 $Å^{-1}$ with three detector configurations (20 m collimation with 8.1 Å neutrons), 12 m (12 m collimation with 5 Å neutrons) and 1.3 m (12 m collimation with 5 Å neutrons). The scattering profiles of the gels were recorded against the scattering vector by using the following equation:

$$q = \frac{4\pi}{\lambda} sin\theta$$

where q is the scattering vector, 2θ is the angle of scattering, λ is the wavelength of the neutron beam. The obtained 2D raw scattering data were reduced and converted to the absolute scale using the Igor Pro software package and Quokka SANS reduction macros (41). Igor Pro was used to subtract appropriate solvent background from each dataset. SasView software version 6.0.1 was used to fit the scattering data.

Ultra-Small Angle Neutron Scattering (USANS)

The USANS data were collected using the Kookaburra Bonse–Hart instrument at ACNS, ANSTO (42). Round demountable cells (40 mm diameter, 1 mm pathlength, 29 mm sample aperture) were used to mount samples. High flux mode was used with a neutron wavelength of 4.74 Å to provide q ranges of 3.5×10^{-5}–0.007 $Å^{-1}$. The experimental USANS data were de-smeared using the Lake algorithm incorporated in NIST USANS macros. SasView was used to fit the scattering data.

Rheology

Rheological characterization was conducted using an Anton Paar MCR 302e rheometer equipped with a parallel plate geometry (25 mm disc, 1 mm gap height, 560 μL hydrogel sample). Oscillatory measurements were performed at 0.2% strain and a frequency of 1 Hz at 37 °C, unless otherwise stated. Gelation time was defined as the crossover point at which the storage modulus (G′) exceeded the loss modulus (G″) during oscillatory time sweep measurements.

Strain sweep tests were conducted with a log ramp up rate from 0.02% shear strain to 200% at 1 Hz within 10 min at 37 °C. Thixotropic tests were conducted by applying 50% shear strain for 4 minutes,

followed by a decrease to 0.1% shear strain for 1 h. Viscosity flow curves were obtained by applying a logarithmic ramp from a shear rate of 0.01 to 10 s^{-1} over a 10-minute period.

View Article Online
DOI: 10.1039/D6TB00490C

Stress relaxation tests were performed at 5% strain for 0.5 h. Stress relaxation data were normalized to the initial maximum stress (σ_0) recorded immediately after application of strain and presented as $\sigma(t)/\sigma_0$. The decay half-time was determined as the time required for stress to decrease to 50% of the initial normalized value.

Cell Culture and seeding

Adipose-derived stem cells (ADSCs; ATCC PCS-500-011) were introduced into the hydrogel systems at a final concentration of 5×10^5 cells/mL for morphometric analysis. The cells were cultured in low-glucose DMEM (Thermo Fisher Scientific 11885084) enriched with 10% fetal bovine serum (FBS, Bovo-Gen, SFBS-AU) and 1% penicillin–streptomycin (Sigma-Aldrich P4333). Routine cultures were kept at 37 °C in a 5% CO_2 atmosphere and only passages 7–10 were used in the experiments. For 3D cell encapsulation within the Trpzip and Trpzip/Trpzip-PEG hydrogels, the cells were detached using 0.05% trypsin, counted, and collected by centrifugation. The resulting pellet was resuspended in the PEG conjugate precursor including media. A volume of 50 µL of this cell–PEG conjugate mixture was dispensed into each well of a 96-well flat-bottom plate including 50 µL of Trpzip precursor to achieve a density of 0.5×10^6 cells/mL to do morphometric analysis for all material formulations. After stabilizing for 1 h, 150 µL of fresh medium was carefully added to each well. All conditions were prepared in triplicate and maintained for two predefined culture durations.

Immunofluorescence Staining and Confocal Imaging

Cell-laden hydrogels were fixed using 4% paraformaldehyde (PFA; Sigma-Aldrich, P6148) at 4 °C overnight. Following fixation, samples were rinsed twice with 1× PBS at 1-h intervals and then kept in PBS at 4 °C until further processing. Cell permeabilization was carried out with 0.1% Triton X-100 overnight. Samples were subsequently blocked in 1% BSA overnight and washed three times with PBS, with each wash separated by 4 h. For staining, hydrogels were incubated with Phalloidin-647 (1:250) and DAPI (1:500) for at least 24 h at 4 °C. After staining, samples were washed three additional times in 1× PBS over a 24 h period and maintained in PBS at 4 °C until imaging.

Confocal microscopy was performed on a Leica SP8 system. A 10× objective with a 2.5 mm working distance was used to enable imaging deeper into the 3D constructs. Z-stack images were acquired at 2.5 µm intervals, generating 50 optical slices at a resolution of 1024 × 1024 pixels. Image processing and quantification were conducted using Fiji (ImageJ).

Cell viability and proliferation assay

To do cell viability assay, the hydrogels were seeded at a final concentration of 2.5×10^5 cells/mL, following the same general procedure described earlier. Cell viability was evaluated after 48 h using a Calcein-AM/Ethidium Homodimer staining kit (Thermo Fisher Scientific, cat. 13224). To perform the live/dead assay, Trpzip and Trpzip–PEG gels were incubated with Calcein-AM (0.5 µL/mL) and Ethidium Homodimer-1 (2 µL/mL) for 40 minutes. Following staining, the samples were rinsed three times with PBS to remove excess dye before imaging.

Cell proliferation within the hydrogel constructs was quantified using the CyQUANT® GR assay following the manufacturer's instructions. At each time point (Day 0, 1, and 7), ADSCs encapsulated in the hydrogels were retrieved by mechanically dissociating the gels through repeated pipetting in culture medium. The suspensions were collected in Eppendorf tubes and centrifuged to obtain a cell pellet. For each sample, the pellet was resuspended in 200 µL of supernatant mixed with CyQUANT® GR dye (Component A, diluted 1:400 in molecular-grade water) and cell-lysis buffer (Component B, diluted 1:20), and transferred into a black 96-well plate. Samples were incubated for 2 h at room temperature to allow complete dye uptake and fluorescence development.

Fluorescence was measured using a CLARIOstar Plus microplate reader (BMG LABTECH) with an excitation wavelength of 480 nm and emission at 520 nm. Each hydrogel formulation was assessed in triplicate, and values were compared with their corresponding Day 0 controls. Relative cell proliferation was expressed as the ratio of fluorescence intensity between treated samples and their Day 0 controls, where *F*represents the relative fluorescence units (RFU). Fold change in proliferation was calculated as $F_{\text{treated}}/F_{\text{control}}$, with values greater than 1 indicating increased proliferation and values below 1 indicating reduced cell growth (43,44).

A minimum of 9 randomly selected images from different regions of each sample were analyzed to quantify the number of live and dead cells using ImageJ software. Cell viability was subsequently calculated as the percentage of live cells relative to the total cell count.

Statistical Analysis

All statistical analyses and plotting of all data were carried out using GraphPad Prism (version 10.3.1). Experiments were conducted with a minimum sample size of $n \geq 3$. Results are presented as mean ± standard deviation (SD). Post-hoc comparisons among multiple groups were performed using one-way ANOVA followed by Tukey's multiple comparisons test. Statistical significance was defined as $*p < 0.05$, $**p < 0.01$, and $***p < 0.001$.

Author contributions

S.T. and K.A.K. conceived and initiated the study. S.T. performed the experiments, analyzed the data, prepared the figures, and coordinated the manuscript preparation. M.S.I. contributed to the cell-based experiments, data analysis, and manuscript revision. R.B.D. and J.M. contributed to the collection of SANS and USANS data and analysis. A.K.N. and J.R. performed cryo-TEM imaging. S.T., M.S.I., R.D.T., and K.A.K. contributed to manuscript writing, with input from all authors. K.A.K. supervised the project and provided funding support.

Conflicts of interest

There are no conflicts to declare.

Acknowledgements

This work was supported through funding from the Australian Research Council Grant DP230101804 (K.A.K.) and NSW Health through a Cardiovascular Research Capacity Program Senior Researcher Grant (K.A.K.). The authors gratefully acknowledge ANSTO's support in providing access to instruments, capabilities and facilities for neutron scattering as outlined in Proposal P-19102. Furthermore, the work benefitted from SasView SANS/USANS modelling software originally developed under NSF award DMR-0520547.The authors acknowledge the help and support of staff at the Katharina Gaus Light Imaging Facility (KGLMF) and Electron Microscopy Unit (EMU) of the UNSW Mark Wainwright Analytical Centre.

Reference

1. Afewerki S, Sheikhi A, Kannan S, Ahadian S, Khademhosseini A. Gelatin-polysaccharide composite scaffolds for 3D cell culture and tissue engineering: Towards natural therapeutics. Bioeng Transl Med [Internet]. 2019 Jan 28;4(1):96–115. Available from: https://aiche.onlinelibrary.wiley.com/doi/10.1002/btm2.10124
2. Nguyen AK, Molley TG, Kardia E, Ganda S, Chakraborty S, Wong SL, et al. Hierarchical assembly of tryptophan zipper peptides into stress-relaxing bioactive hydrogels. Nat Commun. 2023;14(1).
3. Prendergast ME, Davidson MD, Burdick JA. A biofabrication method to align cells within bioprinted photocrosslinkable and cell-degradable hydrogel constructs via embedded fibers. Biofabrication. 2021;13(4).
4. González-Díaz EC, Varghese S. Hydrogels as extracellular matrix analogs. Gels. 2016;2(3).
5. Khine YY, Stenzel MH. Materials Horizons Surface modified cellulose nanomaterials : a source of non-spherical nanoparticles for drug delivery. 2020;
6. Saunders L, Ma PX. Self-Healing Supramolecular Hydrogels for Tissue Engineering Applications. Macromol Biosci [Internet]. 2019 Jan 22;19(1). Available from:

https://onlinelibrary.wiley.com/doi/10.1002/mabi.201800313

7. Gattazzo F, Urciuolo A, Bonaldo P. Biochimica et Biophysica Acta Extracellular matrix : A dynamic microenvironment for stem cell niche ☆. BBA - Gen Subj [Internet]. 2014;1840(8):2506–19. Available from: http://dx.doi.org/10.1016/j.bbagen.2014.01.010
8. Distler T, Boccaccini AR. Acta Biomaterialia 3D printing of electrically conductive hydrogels for tissue engineering and biosensors – A review. Acta Biomater [Internet]. 2020;101:1–13. Available from: https://doi.org/10.1016/j.actbio.2019.08.044
9. Li Y, Kilian KA. Bridging the Gap : From 2D Cell Culture to 3D Microengineered Extracellular Matrices. 2015;2780–96.
10. Hinton TJ, Jallerat Q, Palchesko RN, Park JH, Grodzicki MS, Shue HJ, et al. Three-dimensional printing of complex biological structures by freeform reversible embedding of suspended hydrogels. Sci Adv. 2015;1(9).
11. Barber BE, Jamieson EMG, White LEM, McTernan CT. Embracing Complexity: Peptides as Tunable Scaffolds in the Construction of Discrete Supramolecular Systems. Angew Chemie - Int Ed. 2025;202512014.
12. Su X, Yang B, Chen L, Liu Q, Liu A, Tan ML, et al. REMOVED: Peptide-based co-assembling materials: Bridging fundamental science and versatile applications. Prog Mater Sci. 2025;156(August 2025):101500.
13. Zhang H, Wang J, Wei J, Fu X, Ma J, Chen J. Molecular Engineering of Recombinant Protein Hydrogels: Programmable Design and Biomedical Applications. Gels [Internet]. 2025 Jul 26;11(8):579. Available from: https://www.mdpi.com/2310-2861/11/8/579
14. Wu C, Liao W, Zhang Y, Yan Y. Peptide-based supramolecular hydrogels and their biotherapeutic applications. Biomater Sci. 2024;12(19):4855–74.
15. Lee S, Trinh THT, Yoo M, Shin J, Lee H, Kim J, et al. Self-assembling peptides and their application in the treatment of diseases. Int J Mol Sci. 2019;20(23).
16. Liao H shun, Lin J, Liu Y, Huang P, Jin A, Chen X. from peptide amphiphiles in solution and. 2016;14814–20.
17. Yang L, Gan S, Guo Q, Zhang H, Chen Q, Li H, et al. Stimuli-controlled peptide self-assembly with secondary structure transitions and its application in drug release. Mater Chem Front. 2021;5(12):4664–71.
18. Das S, Das D. Rational Design of Peptide-based Smart Hydrogels for Therapeutic Applications. Front Chem. 2021;9(November):1–30.
19. Clarke DE, Pashuck ET, Bertazzo S, Weaver JVM, Stevens MM. Self-Healing, Self-Assembled β-Sheet Peptide–Poly(γ-glutamic acid) Hybrid Hydrogels. J Am Chem Soc [Internet]. 2017 May 31;139(21):7250–5. Available from:

https://pubs.acs.org/doi/10.1021/jacs.7b00528

20. Liu J, Lou X, Schotman MJG, Marín San Román PP, Sijbesma RP. Photo-Crosslinked Coumarin-Containing Bis-Urea Amphiphile Hydrogels. Gels. 2022;8(10).

21. Liu YS, Chakravarthy RD, Saddik AA, Mohammed M, Lin HC. Supramolecular polymer/peptide hybrid hydrogels with tunable stiffness mediated by interchain acid-amide hydrogen bonds. RSC Adv. 2022;12(22):14315–20.

22. Segneanu AE, Bejenaru LE, Bejenaru C, Blendea A, Mogoşanu GD, Biţă A, et al. Advancements in Hydrogels: A Comprehensive Review of Natural and Synthetic Innovations for Biomedical Applications. Polymers (Basel). 2025;17(15):2026.

23. Holz E, Darwish M, Tesar DB, Shatz-Binder W. A Review of Protein- and Peptide-Based Chemical Conjugates: Past, Present, and Future. Pharmaceutics. 2023;15(2).

24. Nguyen AK, Islam S, Doshi RB, Yu M, Romanazzo S, Ruan J, et al. Tuning Embryoid Germ Layer Specification in Tryptophan Zipper Hydrogels Through Pendant Matrix-Derived Motifs. 2025;03600:1–12.

25. Liu Y, Islam MS, Bakker A, Li Z, Ajam A, Kruzic JJ, et al. Improving the bioactivity and mechanical properties of poly(ethylene glycol)-based hydrogels through a supramolecular support network. J Mater Chem B. 2024;1286–95.

26. Doshi R, Mohanathas D, Islam MS, Ruan J, Tilley RD, Kilian KA. Biomimetic Hydrogels from Mixed Gellan Gum and Tryptophan Zipper Self-Assembling Peptides. ACS Macro Letters. 2025 May 9.

27. Camacho P, Fainor M, B. Seims K, W. Tolbert J, W. Chow L. Fabricating spatially functionalized 3D-printed scaffolds for osteochondral tissue engineering. J Biol Methods. 2021;8(1):1.

28. Hule RA, Nagarkar RP, Altunbas A, Ramay HR, Branco MC, Schneider JP, et al. Correlations between structure, material properties and bioproperties in self-assembled β-hairpin peptide hydrogels. Faraday Discuss. 2008;139:251–64.

29. Zhang S. Fabrication of novel biomaterials through molecular self-assembly. Nat Biotechnol. 2003;21(10):1171–8.

30. Clarke DE, Pashuck ET, Bertazzo S, Weaver JVM, Stevens MM. Self-Healing, Self-Assembled β-Sheet Peptide-Poly(γ-glutamic acid) Hybrid Hydrogels. J Am Chem Soc [Internet]. 2017 May 31;139(21):7250–5. Available from: https://pubs.acs.org/doi/10.1021/jacs.7b00528

31. Ishikawa S, Sakai T. One-Pot Approach to Synthesize Tough and Cell Adhesive Double-Network Hydrogels Consisting of Fully Synthetic Materials of Self-Assembling Peptide and Poly(ethylene glycol). ACS Appl Bio Mater. 2023;6(12):5282–9.

32. Pedersen JS, Simulations MC. Scattering Functions of Semiflexible Polymers with and without Excluded Volume Effects. 1996;9297(96):7602–12.
33. Chen W ren, Butler PD, Magid LJ. Incorporating Intermicellar Interactions in the Fitting of SANS Data from Cationic Wormlike Micelles. 2006;(5):6539–48.
34. Feigin LA SD. Structure Analysis by Small-Angle X-Ray and Neutron Scattering. 1987.
35. Otter R, Besenius P. Biomolecular Chemistry. 2019;6719–34.
36. Hamley IW. PEG–Peptide Conjugates. Biomacromolecules [Internet]. 2014 May 12;15(5):1543–59. Available from: https://pubs.acs.org/doi/10.1021/bm500246w
37. Rivas M, Alem C, Puiggal J. Peptide Self-Assembly into Hydrogels for Biomedical Applications Related to Hydroxyapatite. 2019;1–29.
38. Daly AC. Granular Hydrogels in Biofabrication: Recent Advances and Future Perspectives. Adv Healthc Mater. 2023;2301388:1–19.
39. Badescu G, Bryant P, Swierkosz J, Khayrzad F, Pawlisz E, Farys M, et al. A new reagent for stable thiol-specific conjugation. Bioconjug Chem. 2014;25(3):460–9.
40. Wood K, Mata JP, Garvey CJ, Wu CM, Hamilton WA, Abbeywick P, et al. The pinhole small-angle neutron scattering instrument at the OPAL Research Reactor, Australia: design, performance, operation and scientific highlights. J Appl Crystallogr. 2018;51(2):294–314.
41. Kline SR. Reduction and Analysis of SANS and USANS Data Using IGOR Pro. J Appl Crystallogr. 2006;39(6):895–900.
42. Rehm, C.; Brûlé, A.; Freund, A. K.; Kennedy SJK. The Ultra-Small-Angle Neutron Scattering Instrument at OPAL. J Appl Cryst. 2013;46(6):1699–1704.
43. Chowdhuri S, Saha A, Pramanik B, Das S, Dowari P, Ukil A, et al. Smart Thixotropic Hydrogels by Disulfide-Linked Short Peptides for Effective Three-Dimensional Cell Proliferation. Langmuir. 2020;36(50):15450–62.
44. Eriksson J. Investigation of nanocellulose- based hydrogels as scaffolds for cell-delivery to chronic wounds. 2022;

View Article Online
DOI: 10.1039/D6TB00490C

View Article Online
DOI: 10.1039/D6TB00490C

This study generated data including shear rheology, spectroscopy, and neutron scattering files which are stored in instrument specific software formats and in ASCII file formats, and microscopy files and images.

The datasets generated during the current study are not publicly available due to further analysis related to future publications but are available from the corresponding author on reasonable request.